Thin Solid Films 527 (2013) 31–37

Contents lists available at SciVerse ScienceDirect

Thin Solid Films

journal homepage: www.elsevier.com/locate/tsf

Graphene production by dissociation of camphor molecules on nickel substrate

Fotini Ravani [a,b], Konstantinos Papagelis [a,c], Vassileios Dracopoulos [a], John Parthenios [a], Konstantinos G. Dassios [a,d], Angeliki Siokou [a], Costas Galiotis [a,b,c,*]

[a] Foundation of Research & Technology — Hellas, Institute of Chemical Engineering Sciences (FORTH/ICE-HT), 26504, Patras, Greece
[b] Interdepartmental Program in Polymer Science and Technology, University of Patras, 26504, Patras, Greece
[c] Department of Materials Science, University of Patras, 26504, Patras, Greece
[d] Department of Material Science and Engineering, University of Ioannina, 45110, Ioannina, Greece

ARTICLE INFO

Article history:
Received 21 May 2012
Received in revised form 4 December 2012
Accepted 5 December 2012
Available online 22 December 2012

Keywords:
Graphene
Chemical vapor deposition
Raman spectroscopy
Camphor

ABSTRACT

A chemical vapor deposition (CVD) process for the production of continuous-high quality-graphene layers based on camphor decomposition on polycrystalline Ni foil, is demonstrated. In situ X-ray diffraction at the pyrolysis temperature of the Ni foil indicates the presence of dominant Ni <111> grains which play an important role in the carbon nucleation and growth. The topography of the grown graphene layers is studied by scanning electron microscopy and atomic force microscopy which show that the Ni surface is covered by continuous and wrinkled graphene carpets. Raman spectroscopy reveals the high quality of the graphene film which appears to be only a few monolayers thick. X-ray photoelectron spectroscopy indicates the existence of graphitic layers and the absence of any spectral features associated with carbides (Ni_xC). The proposed CVD process is a sufficient method for large scale production of graphene films.

1. Introduction

Graphene consists of carbon atoms in sp^2 bonding hybridization, arranged in a honeycomb lattice. Its extraordinary properties can have a number of applications in various fields such as nano- and bio-electronics, liquid crystal devices and ultracapacitors [1]. Geim and Novoselov [2] isolated graphene flakes of high structural quality but of small dimensions. The produced graphene flakes were isolated by the mechanical exfoliation of bulk highly oriented pyrolitic graphite, using the scotch tape technique. Motivated by the superior properties of graphene [3] and the low yield of the exfoliation methods, different processes are currently under development that aim to increase the production yield but also to deliver flakes of larger dimensions. Chemical wet etching of graphite with various treatments based on Hummers and Offeman methods [4] is an alternative approach to obtain graphene but with the presence of both oxidized carbon and structural defects on the graphene hexagonal lattice. More advanced plasma-enhanced chemical etching of graphite, leads also to the formation of higher quality graphene but still residual oxygen functional groups remain on graphene's surface [5]. A quite different approach for graphene production is the epitaxial growth on either Si or C terminated SiC single crystal surfaces after thermal decomposition of SiC due to evaporation of Si atoms [6]. This method results in wafer-scale graphene fabrication and for this reason is quite appealing for the microelectronics industry. However, the cost of single SiC crystal wafers and the very high temperature required for silicon evaporation are still important impediments for the industrial exploitation of this method.

A promising approach for the epitaxial growth of graphene is the chemical vapor deposition (CVD) of organic gasses onto appropriate catalytically active substrates. Carbon nanotubes and nanofibers have already been produced via appropriate CVD processes [7]. By introducing transition metal foils [8] in order to lower the energy barriers for thermal decomposition of carbon clusters and graphene growth, the quality of the graphene layers may approach the requirements of the semiconductor industry. While CVD grown graphene with dimensions of about cm^2 has been achieved on the above metal surfaces, wafer scale graphene areas exhibiting thicknesses ranging from one to few graphene layers have been mostly realized on Cu and Ni surfaces. For example, Ruoff et al. [9] demonstrated a copper catalyzed CVD process, in which by annealing gas mixture of methane and hydrogen at 1000 °C, large scale graphene islands with thickness of up to 3 monolayers are produced on copper substrates. Using a similar CVD process but with a polycrystalline Ni foil as a catalyst, ultrathin (up to 10 monolayers) continuous graphene films have been obtained by Reina et al. [10].

Transition metal assisted CVD graphene production by source gasses such as versatile ratios of CH_4/H_2 [11] or/and Ar [12] and C_2H_2/H_2 [13] has been reported over the last few years. These processes were carried out under high vacuum [12] or under ambient conditions [10] and from relatively high cooling rates [13] up to room temperature. However, with regards to carbon source for CVD fabrication there have been limited reports in the literature. Somani et al. [14] reported graphene

---

[*] Corresponding author at: Department of Materials Science, University of Patras, 26504, Patras, Greece. Tel.: +30 2610 965 301; fax: +30 2610 965 275.
E-mail address: c.galiotis@iceht.forth.gr (C. Galiotis).

0040-6090/$ – see front matter © 2012 Elsevier B.V. All rights reserved.
http://dx.doi.org/10.1016/j.tsf.2012.12.029

synthesis from pyrolysis (850 °C) of camphor in Ar atmosphere on Ni surface, resulting to disorder graphitic structure with thickness of about 35 graphene monolayers. An alternative camphor based CVD synthesis which produced multi layer graphene domains of about ~1 μm wide and with an average thickness up to 13 layers was reported recently [15]. The same group had also proposed a modification of the above CVD method on Cu foil [16] but at higher temperature (1020 °C) for the production of few-layer-graphene (up to 3–4 layers). Moreover, thin films of spin-coated poly (methyl metha-crylate) (PMMA) [17], on metal surface have also been used as a solid carbon source by CVD. In this case, the growth of graphene layers is obtained by a reductive gas flow of H_2/Ar.

Comparing the two volatile solid carbon precursors such as the PMMA and camphor mentioned above, the latter has the advantage of being a natural hydrocarbon whereas PMMA is an acrylic polymer produced through a relatively complex chemical route [18]. Another aspect worth mentioning is the necessity of using H_2 for the PMMA-based CVD process which can be considered as a drawback due to the high flammability of H_2 in the presence of oxygen. Furthermore, graphene formation on Ni foil is a well-known industrial heterogeneous catalysis process [19] and camphor, being a renewable feedstock, is an abundant and inexpensive carbon source [7]. Hence, production of graphene by CVD on a Ni foil using camphor is a viable alternative for fabrication at an industrial scale.

In this work, an efficient, low temperature (850 °C) and cost effective CVD process is employed, utilizing camphor as a solid precursor. The desired thickness of graphene films is achieved by turning off the heat and letting the system to cool down to room temperature on its own (estimated cooling rate up to 550 °C: 8 °C/min). This should be contrasted with the rather laborious flash cooling rates reported in the literature [13]. The produced graphene is characterized by means of a variety of analytical techniques such as scanning electron microscopy (SEM), X-ray photoelectron spectroscopy (XPS), atomic force microscopy (AFM) and Raman. In-situ high temperature (HT) X-ray diffraction (XRD) and electron backscatter diffraction (EBSD) measurements revealed the Ni surface morphology during annealing. The crystal quality and thickness of the formed graphene layers is investigated by Raman and X-ray photoelectron spectroscopies. The optimization of relevant parameters for graphene production such as camphor quantity and the deposition time could provide us a fine control of the thickness and structure of graphene.

2. Experimental details

2.1. Production of graphene layers

The CVD reactor was a quartz tube (length: 1 m, inner diameter: 4 cm) in which a polycrystalline Ni foil (99% purity by Aldrich), was placed. The tube was placed into a three-zone furnace which could be heated up to 1100 °C. The Ni substrate (1 cm × 1 cm) was polished by chemical–mechanical polishing before its introduction into the reactor. The CVD process consisted of two steps. Initially, a small quantity of camphor ($C_{10}H_{16}O$) in powder form was annealed at 200 °C and evaporated in the reactor. Then, using Ar as an inert carrier gas, the camphor molecules from the vapor phase flowed in the CVD reactor and were pyrolysed at 850 °C. The Ar gas flow rate was kept at a constant value of 800 ml/min. After 5 min of camphor decomposition the substrate was cooled down to room temperature at a rate of 8 °C/min (up to 550 °C) under an Ar atmosphere. Both steps are illustrated in Fig. 1 in which a sketch of the proposed CVD process is presented.

2.2. Characterization

2.2.1. X-ray photoelectron spectroscopy

XPS was used to examine the surface chemistry of the decomposed camphor molecules onto the polished polycrystalline Ni surface. The XPS measurements were carried out in an ultra high vacuum system equipped with a SPECS LHS-10 hemispherical electron analyzer using unmonochromatized MgKα (1253.6 eV) line. For a constant analyzer pass energy of $E_p = 36$ eV the full width at half maximum (FWHM) of the C1s XPS peak was 1 eV. The C1s peak was deconvoluted by Gaussian–Lorentzian components following a Shirley background subtraction.

2.2.2. Raman spectroscopy

MicroRaman (InVia Reflex, Rensihaw, UK) spectra were recorded with the 514.5 nm (2.41 eV) excitation, while the laser power was kept below 1 mW to avoid laser induced local heating on the studied samples. A × 100 objective with numerical aperture of 0.9 was used. All peaks in the Raman spectra of graphene were fitted with Lorentzians. The 2D linewidths together with 2D/G relative intensities were used to identify graphene monolayers.

2.2.3. X-ray diffraction

XRD measurements from the nickel substrate were carried out in a Bruker D8 ADVANCE diffractometer operating in θ–θ Bragg–Brentanno geometry. A high temperature furnace (XRK900, Anton Paar GmbH) was attached on the diffractometer in order to record diffractograms at elevated temperatures. The temperature was controlled through a temperature control unit (TCU750 Anton Paar GmbH) and was increased to 850 °C with a step of 5 °C/min and maintained there for 5 min in order to ensure temperature homogeneity over the sample. Then the system was cooled down to room temperature. During the thermal cycle the sample was under inert Ar atmosphere. Diffractograms were collected in the temperature range 25–850 °C, while at each temperature the beam was aligned in order to minimize instrument effects in the peak shapes and intensities. A CuK_a radiation source was used, operating at 40 kV and 40 mA, while the diffracted beam was collected with 1-D SSD LynxEye detector. Diffraction patterns were recorded in a continuous mode between 20° and 95° in the 2θ range with a step size 0.02° and scan time of 0.5 s/step.

2.2.4. Scanning electron microscopy

The morphology of the grown graphene samples on the Ni substrate was studied with variable pressure scanning electron microscope having a field emission gun (Zeiss SUPRA 35VP) operating at 15 kV. Grain size and orientation before and after the heat treatment of the substrate was measured with an EBSD system (HKL Nodlys II) attached on the SEM microscope. The accelerating voltage of the primary beam for the backscattered images was at 30 kV at a working distance of 15 mm and an aperture of 120 μm. EBSD 600 μm × 600 μm maps (300 × 300 points; step = 2 μm) were collected from different areas of the sample and analyzed by the TANGO software.

2.2.5. Atomic force microscopy

AFM was employed to assess the surface topography of the specimens. The instrument was operated at a tapping mode which employs a constant force method (i.e. the force between the sample surface and the AFM tip was kept constant by a feedback system while the surface beneath the tip was scanned). All specimens were imaged with the aid of multimode scanning probe microscopy (Veeco), using a nanoscope IIIa controller and a 120 μm × 120 μm magnet-free scanner (model AS-130VMF) developed by digital instruments with vertical range 5 μm and z-axis resolution 0.05 nm. The scan rate was 1 Hz. The cantilever's spring constant was 40 N/m. The shape of the silicon nitride tips was square pyramidal with radius of curvature ~10 nm and half angle ~15°. The images were processed with a linear plane fit in order to remove any sample tilt on them.

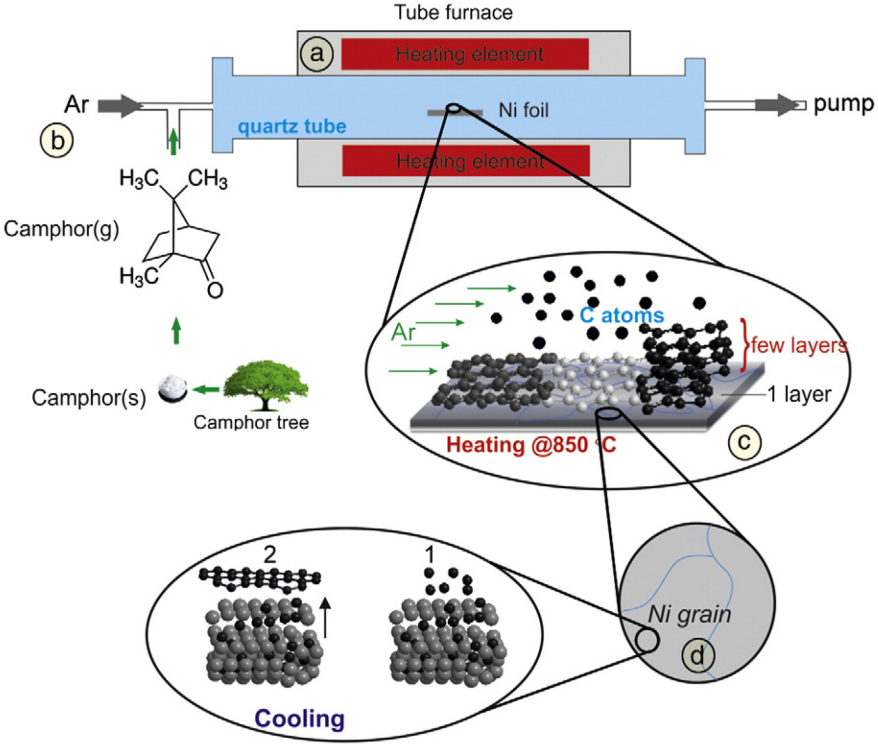

Fig. 1. Schematic of the proposed CVD process for graphene growth on polished polycrystalline Ni substrate. (a) The CVD reactor. (b) Transformation of solid camphor (s) to camphor vapor phase and delivering of camphor molecules to CVD reactor by Ar gas flow. (c) Catalytic decomposition of camphor to carbon atoms (d1). Dissolution of carbon atoms to Ni bulk at elevated temperatures. (d2). Precipitation out of carbon atoms to Ni surface, during cooling down.

3. Results

In Fig. 2 the diffractograms from the Ni substrate obtained at room and elevated (850 °C) temperatures are presented. Direct comparison with the XRD pattern of a standard Ni powder sample (JPDCS No: 00-004-0850) reveals that the Ni substrate has a preferential orientation at both temperatures (Table 1); at 850 °C the peak referred to <111> orientation becomes more intense. Even though the texture of the sample cannot be derived from the 1-D diffractogram a qualitative view of the substrate can be provided. At 850 °C the position of the diffraction peaks is shifted to lower angles due to the thermal expansion of the Ni substrate. The lattice constant was calculated for the respective temperature by the DIFFRAC^{plus} EVA software (BRUKER AXS GmbH). The cubic unit cell was found to expand by ~1.3% in excellent agreement with the literature reported value [20]. In addition to the above, the FWHM of the diffraction peaks is reduced at elevated temperatures, which implies an enhancement of the crystallite and/or grain size. The increased crystallite sizes can be better observed from the forescatter detector images obtained in the field emission (FE)-SEM microscope.

In Fig. 3(a) and (c) the grain morphology before and after the heat treatment in the XRD furnace is presented, respectively. From the comparison of these images it seems that while the grain size of Ni increases after annealing, the orientation of the grains does not change considerably (colored part of Fig. 3(b) and (d)). The substrate <111> orientation is the preferred orientation for graphene growth since the mismatch (1.2%) between the lattice constants of graphene and Ni <111> is negligible. However, recent data obtained from scanning tunneling microscopy (STM) images [21], show that the orientation of the grains is not so crucial since the graphene layer can be formed also on the <110> plane of Ni. Furthermore, the EBSD maps of the annealed Ni substrate (Fig. 3) outlined the dominant role of both the <111> and <110> planes in graphene nucleation and growth on the polycrystalline Ni surface. This finding in conjunction with the SEM micrographs (Fig. 4(a)) confirms that the crystal orientation of Ni does not play a predominant role on graphene formation.

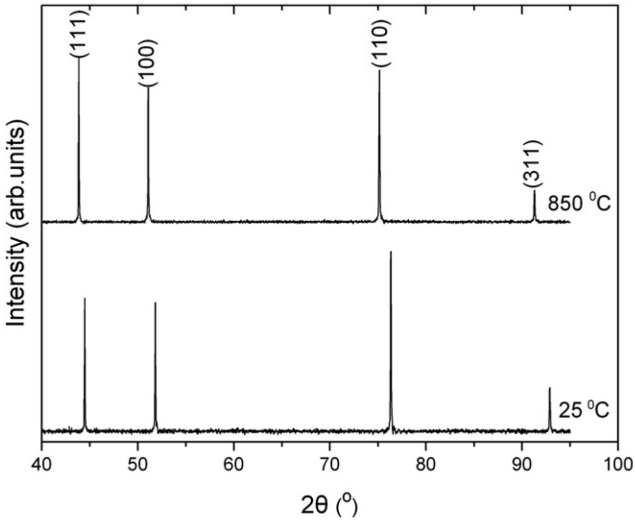

Fig. 2. XRD patterns of polycrystalline Ni foil at 25 °C and 850 °C.

Table 1
Intensity ratios of different orientations for standard Ni powder sample and for Ni foil at room (RT) and high (HT) temperature.

	Reference Ni sample[a]	Experimental results	
Intensity ratio	Ni powder sample	Ni foil at RT	Ni foil at HT
I (111)/I(100)	2.38	0.9	1.02
I (111)/I(110)	4.76	0.57	0.68
I (111)/I(311)	5	2	2.97

[a] JPDCS No: 00-004-0850.

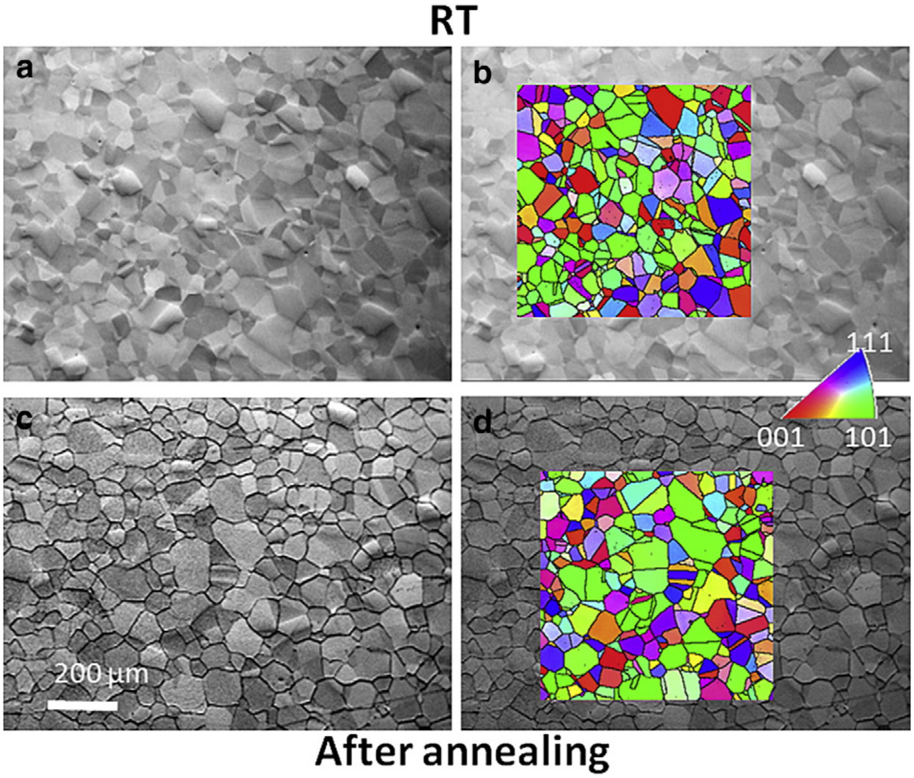

Fig. 3. EBSD maps obtained for polycrystalline Ni foil before and after annealing. (a) Forescatter image before annealing. (b) EBSD orientation map overlay to the forescatter image (a). (c) Forescatter image after annealing. (d) EBSD orientation map overlay to the forescatter image (c).

Catalytic decomposition of camphor molecules leads to a continuous coverage of graphene films on the above studied polycrystalline Ni surface. SEM images in Fig. 4 show that the produced graphene films are wrapped as carpets on the polished Ni surface of the grain boundaries (white dashed arrows) which are visible underneath the graphene carpets. The wrinkled feature of the carpets is due to the accommodation of the thermal expansion difference between the Ni substrate and graphene [22]. In Fig. 4(a) the solid arrows target these wrinkles which resemble ridges of the formed graphene tissue. Furthermore, dark gray colored areas, which are marked with symbol A, represent thicker graphene domains [23]. This dispersion of thinner and thicker neighboring areas results to a heterogeneous coverage of graphene layers on Ni surface. The AFM image shown in Fig. 5(a) further justifies the buckled graphene surface topology. Fig. 5(b) shows the cross section height profile corresponding to the line of Fig. 5(a). The measured height of the formed wrinkles is about 30 nm in accordance with the STM data [24]. Also, in Figs. 4(a) and 5(a) almost spherical shaped carbon structures are randomly deposited on graphene surface. The condensation of organic molecules (camphor) from the gas phase upon cooling seems to be a plausible explanation for the origin of these structures.

Fig. 4(b)–(d) illustrates SEM images of free-standing few-layer graphene, which are probably segments of the material that have been broken off from the main body of the carpet following the release of thermal stress. The size of the stacked free-standing graphene sheets in Fig. 4(b)–(c) ranges from 1 to 5 µm. The ultrathin transparent graphene films with size up to 0.7 µm are illustrated in Fig. 4(d) while in the background low height darkened ridged features are formed. Furthermore, well-shaped hexagonal domains reflecting the hexagonal graphitic structure are clearly presented in Fig. 4(f); the size of the hexagons is estimated to 1.3 µm.

Raman spectroscopy provides a fast and facile structural and quality characterization of graphene-based materials. Fig. 6 presents typical Raman spectra collected from different locations of the synthesized graphene films. The faint-intensity of the disorder-induced D band (~1350 cm^{-1}) confirms that the graphene formed on polycrystalline Ni foil is of low defect density and of high quality. The peaks appeared at ~1584 cm^{-1} and ~2712 cm^{-1} (Table 2) can be assigned to the G and 2D bands of graphene membranes, respectively. As it is evident from Fig. 6 the 2D peak shows a broad almost symmetrical line-shape; the corresponding FWHM ranging from 37 to 55 cm^{-1} (Table 2). It is well known that the 2D peak position experience a blue shift with increasing the number of graphene layers, providing a signature of multilayer graphene [25–27]. Also, with increasing the number of layers the 2D band experiences a significant broadening due to enhancement of the allowed double resonance processes as a result of the splitting of both the in-plane transverse optical (iTO) phonon and electronic branches [28]. Moreover, the relative integrated intensities of the 2D-to G-band, I(2D)/I(G), can be considered as an additional fingerprint for the formation of monolayer/multilayer graphene [10,13,29,30]. The collected spectra (Fig. 6) exhibit I(2D)/I(G) ratio larger than 1.6 suggesting the presence of few layer graphene (<5) in the studied locations. It should be stressed that the doping from the substrate to the graphene layers [31] and the formation of permanent wrinkles (Figs. 4(a) and 5(a)) [32,33] modify the line shape characteristics of the G and 2D peaks making it hard to identify the exact number of few layers present in the interrogated locations of the samples.

XPS is also employed to provide information on the chemical state of the surface carbon atoms. The peak of the C1s shown in Fig. 7, is analyzed into three components corresponding to carbon atoms at different chemical environments. The sharp peak at binding energy 284.4 eV represents graphitic carbon [34] while the characteristic feature attributed to defects is observed at 285.4 eV [35]. The partial change of chemical environment from sp^2 in aromatic structure to sp^3 and sp^2 not aromatic structure is an additional reason for the coexistence of defects in the sample. The oxidized states of carbon (C_{ox}) are observed at 289.3 eV. The fingerprint of nickel carbide (Ni_xC) in the photoemission spectra of C1s should appear at binding

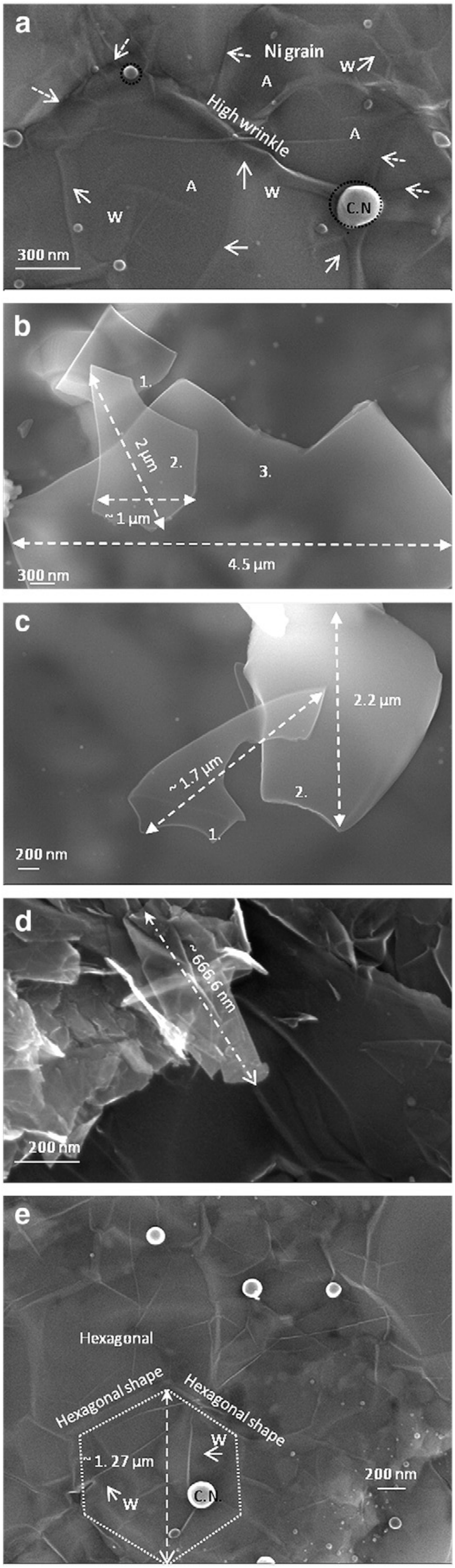

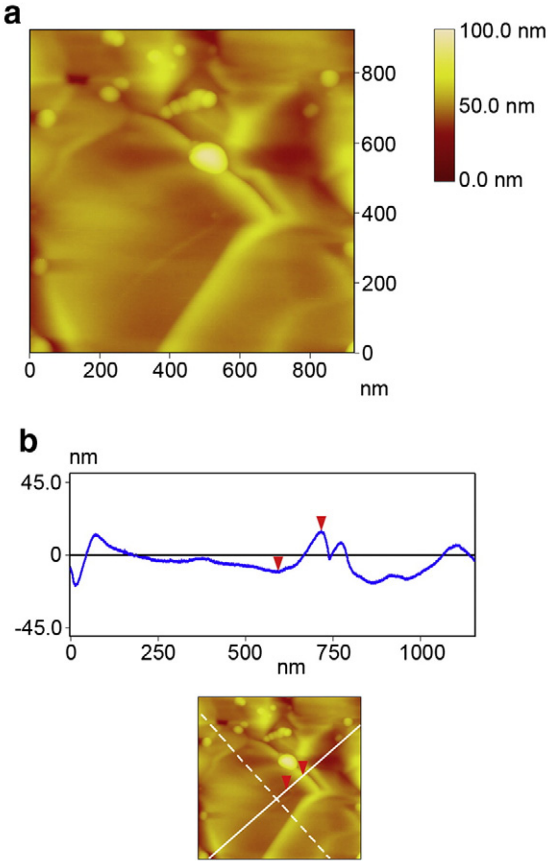

Fig. 5. (a) AFM image of flat and wrinkled graphene carpets on Ni surface. (b) Cross sectional height profile corresponding to the line in (a).

energies lower than 284 eV [36]. It should be added here that the present spectrum does not contain features of carbidic carbon.

4. Discussion: Mechanisms of camphor dissociation on the Ni surface

In the case of Cu substrates, due to the very low carbon solubility into the Cu bulk [37], graphene growth can only be related to the absorption and dissociation of hydrocarbons to intermediate free radicals on the Cu surface. The most widely used carbon source to date is methane [11,12] and in fact the Cu substrate is responsible for its catalytic decomposition that gives rise to active carbon species such as CH_3, CH_2, CH, and C, which subsequently react to produce graphene. The CH_x species on the Cu surface are unstable toward dimerization thus further converging into larger carbonaceous species eventually leading to the most stable graphene. In the methane CVD graphene growth, the presence of H_2 gas plays first an auxiliary catalyst role in the creation of active carbon species and then a key role in the formation of graphitic domains by etching the weak C–C bonds [38]. High methane flow rate is also capable to form continuous large-area graphene films on Cu surface [11]. Moreover the H_2 gas is also useful for reducing the Cu surface as a pretreatment of the catalytic graphene growth. It is evident that in the case of Cu, intermediated carbon species present a more favorable path to graphene growth than through the complete dehydrogenation of CH_4.

Fig. 4. Representative SEM micrographs of the produced graphene films. (a) An extended bouncing of wrinkles (w) is marked with solid arrows. Ni boundaries are marked with dashed arrows. Homogenous coveraged areas are marked with symbol A. Spherical shaped carbon nanostructures are marked with C.N. acronym. (b)–(d) Free standing few layers of graphenes. (e) Well shaped hexagonal domains.

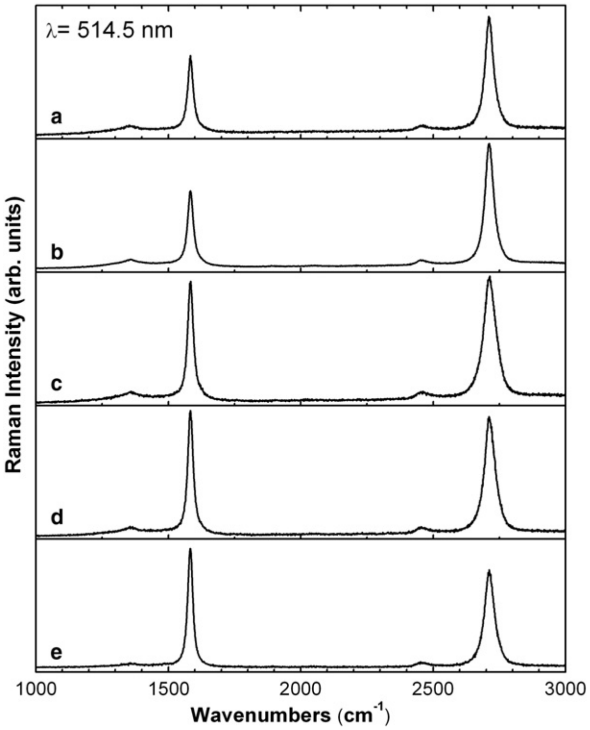

Fig. 6. Typical Raman spectra of the graphene sheets grown on polycrystalline Ni substrate.

The formation of graphene film on the Ni foil occurs as a result of the well-known catalytic activity of Ni [39,40] in decomposing hydrocarbons. As mentioned earlier, camphor was employed here as the carbon source of the CVD process. At the chosen temperature of 850 °C, camphor (g) molecules or its decomposition products from the gas phase (hydrocarbon structures like $C_xH_yO_z$ (g)) absorbed onto the Ni substrate. The absorption is followed by two consecutive steps: (i) the creation of active C_xH_y radicals and atomic carbon and (ii) the dissolution of atomic carbon into the Ni bulk [39] forming a metastable Ni_xC (solid solution) phase. This is in agreement with the binary phase diagrams of Ni and C reported earlier [37,41]. It is worth adding that during annealing the precipitation (from saturated solid solution) onto the Ni surface occurs after some time [42].

Regarding radical formation, the combination of an active catalytic surface and elevated temperatures provides the necessary conditions for the breaking of the sp^3 hybridized carbon atoms and for the subsequent creation of the appropriate active C_xH_y radicals. According to the EBSD maps (Fig. 3(d)) the Ni surface of the proposed CVD process is mainly structured with <110> and <111> orientations which are well known catalytic centers [39]. The active radicals and the precipitated carbon atoms from the solid solution (C_{ss}) start the nucleation of the first graphene layers. The role of hydrogen seems to be crucial for the graphene growth from the formed C_xH_y radicals as it has already been mentioned earlier for the case of the Cu substrate. Moreover in the present CVD method the Ni surface is cleaned out from the physically adsorbed oxygen only with an Ar flow. Although there is no direct experimental evidence for this effect, it has been previously observed to occur even at low temperatures resulting in high purity polycrystalline Ni substrates [43]. As shown in Fig. 1(b) the camphor molecule consists of 10 carbon atoms and 16 hydrogen atoms. The question that now arises is whether the 16 hydrogen atoms of camphor are enough for graphene growth or there is a necessity of an additional source of hydrogen atoms. Since the prior cleaning of Ni excludes any other possible source of hydrogen, we can safely conclude that the camphor is quite adequate as a source for graphene growth. Upon cooling, further segregation of the carbon atoms to the Ni surface takes place (Fig. 1(d2)). The difference in the carbon's chemical environment in graphene and in the Ni bulk induces a chemical potential difference. This is the thermodynamic driving force which causes segregation of C atoms from Ni bulk to Ni surface. Thus, upon cooling, segregation of C_{ss} results in further graphene layer growth to micron size (Fig. 4). Concerning the cooling protocol, it is important to stress that the flash cooling rates are thought to be responsible for the suppression of the precipitating carbon atoms at the Ni surface [44]. In the hereby proposed CVD process the desired thickness of graphene films was achieved by moderate cooling rates (8 °C/min up to 550 °C) and, therefore, there was no need to resort to the flash cooling rates reported earlier [13]. As already mentioned, the average thickness of the formed wrinkled carpets as identified through Raman spectroscopy (Fig. 6), is estimated to just few graphene layers (<5) although the exact value could not be accurately defined. Finally, it is concluded that in contrast to the Cu substrate, the high solubility of C atoms to Ni bulk and not the free radicals plays the most fundamental role in the graphene growth reported in this work.

Table 2
G and 2D peak positions, FWHM and I(2D)/I(G) intensity ratios extracted from the spectra presented in Fig. 6.

Locations	G (cm^{-1})		2D (cm^{-1})		I(2D)/I(G)
	FWHM	Pos	FWHM	Pos	
A	24.6	1584	37.5	2712	2.4
B	25.3	1584	37.9	2712	2.5
C	24.7	1584	55.0	2714	2.3
D	22.9	1584	47.6	2714	2.0
E	22.2	1583	44.8	2712	1.6

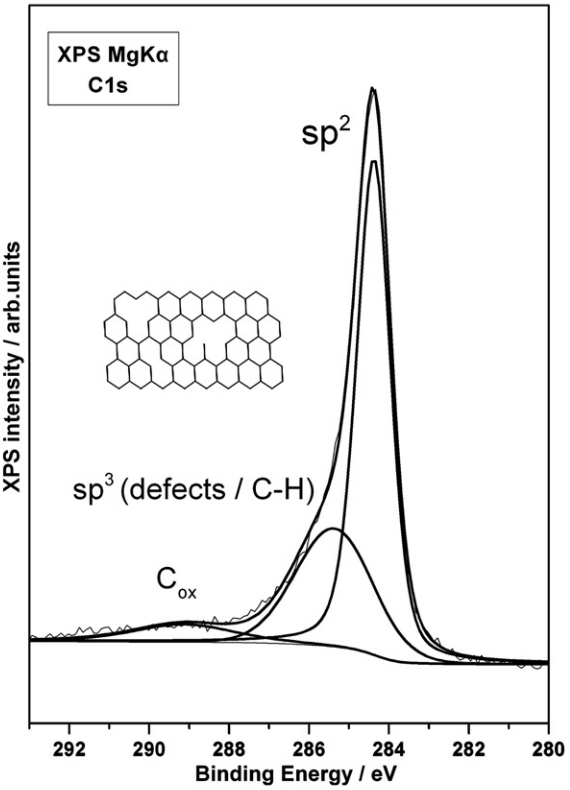

Fig. 7. C1s XPS core level spectra of the graphene sheets on Ni surface.

5. Summary

The use of graphene in practical applications requires inexpensive fabrication methods. Chemical vapor deposition has, in recent years, been recognized as the most promising method for inexpensive production of large-scale graphene. This work moves in this direction since the process temperature decreased from 1000 °C to 850 °C and the hydrocarbon gasses have been replaced by camphor which is an abundant natural solid volatile precursor. Furthermore the present experiments showed that there is neither a necessity for a separate cooling chamber nor a hydrogen gas most probably because the removal of physically absorbed oxygen atoms from the polycrystalline Ni foil is achieved by Ar gas. The produced few-layer graphene flakes were of high quality and scalable (~5 μm). Experimental efforts are currently focused on the production of graphene flakes with controllable thickness.

Acknowledgments

Financial support from the FORTH Graphene Centre and the PHOSIL program (FP7-LEADERA solicited by the Region of Western Greece) is gratefully acknowledged. The authors would also like to thank Dr. Vagelis Karoutsos for conducting the AFM experiments.

References

[1] A.K. Geim, K.S. Novoselov, Nat. Mater. 6 (2007) 183.
[2] K.S. Novoselov, A.K. Geim, S.V. Morozov, D. Jiang, Y. Zhang, S.V. Dubonos, I.V. Grigorieva, A.A. Firsov, Science 306 (2004) 666.
[3] O. Frank, G. Tsoukleri, I. Riaz, K. Papagelis, J. Parthenios, A.C. Ferrari, A.K. Geim, K.S. Novoselov, C. Galiotis, Nat. Commun. 2 (2011) 255.
[4] W.S. Hummers, R.E. Offeman, J. Am. Chem. Soc. 80 (1958) 1339.
[5] G. Zhao, D. Shao, C. Chen, X. Wang, Appl. Phys. Lett. 98 (2011) 183114.
[6] S.N. Yanopoulos, A. Siokou, N.K. Nasikas, V. Dracopoulos, F. Ravani, G.N. Papatheodorou, Adv. Funct. Mater. 22 (2012) 113.
[7] M. Kumar, Y. Ando, J. Nanosci. Nanotechnol. 10 (2010) 3739.
[8] M. Batzill, Surf. Sci. Rep. 67 (2012) 83.
[9] X. Li, W. Cai, J. An, S. Kim, J. Nah, D. Yang, R. Piner, A. Velamakanni, I. Jung, E. Tutuc, S.K. Banerjee, L. Colombo, R.S. Ruoff, Science 324 (2009) 1312.
[10] A. Reina, X. Jia, J. Ho, D. Nezich, H. Son, V. Bulovic, M.S. Dresselhaus, J. Kong, Nano Lett. 9 (2009) 130.
[11] X. Li, C.W. Magnuson, A. Venugopal, J. An, J.W. Suk, B. Han, M. Borysiak, W. Cai, A. Velamakanni, Y. Zhu, L. Fu, E.M. Vogel, E. Voelkl, L. Colombo, R.S. Ruoff, Nano Lett. 10 (2010) 4328.
[12] A. Robertson, J.H. Warner, Nano Lett. 11 (2011) 1182.
[13] S.J. Chae, F. Güneş, K.K. Kim, E.S. Kim, G.H. Han, S.M. Kim, H.J. Shin, S.M. Yoon, J.Y. Choi, M.H. Park, C.W. Yang, D. Pribat, Y.H. Lee, Adv. Mater. 21 (2009) 2328.
[14] P.R. Somani, S.P. Somani, M. Umeno, Chem. Phys. Lett. 430 (2006) 56.
[15] G. Kalita, M. Masahiro, H. Uchida, K. Wakita, M. Umeno, Mater. Lett. 64 (2010) 2180.
[16] G. Kalita, K. Wakita, M. Umeno, Phys. E 43 (2011) 1490.
[17] Z. Sun, Z. Yan, J. Yao, E. Beitler, Y. Zhu, J.M. Tour, Nature 468 (2010) 549.
[18] C. Loubat, S. Soulier, B. Boutevin, Polym. Bull. 45 (2001) 487.
[19] J. Wintterlin, M.-L. Bocquet, Surf. Sci. 603 (2009) 1841.
[20] G. Odahara, S. Otani, C. Oshima, M. Suzuki, T. Yasue, T. Koshikawa, Surf. Interface Anal. 43 (2011) 1491.
[21] Y. Murata, V. Petrova, B.B. Kappes, A. Ebnonnasir, I. Petrov, Y.-H. Xie, C.V. Ciobanu, S. Kodambaka, ACS Nano 4 (2010) 6509.
[22] S. Amini, H. Kalaantari, J. Garay, A.A. Balandin, A. Reza, J. Mater. Sci. 46 (2011) 6255.
[23] H.J. Park, J. Meyer, S. Roth, V. Ska´kalova, Carbon 48 (2010) 1088.
[24] A.N. Obraztsov, E.A. Obraztsova, A.V. Tyurnina, A.A. Zolotukhin, Carbon 45 (2007) 2017.
[25] A.C. Ferrari, J.C. Meyer, V. Scardaci, C. Casiraghi, M. Lazzeri, F. Mauri, S. Piscanec, D. Jiang, K.S. Novoselov, S. Roth, A.K. Geim, Phys. Rev. B 97 (2006) 187401.
[26] A. Gupta, G. Chen, P. Joshi, S. Tadigadapa, P.C. Eklund, Nano Lett. 6 (2006) 2667.
[27] D. Graf, F. Molitor, K. Ensslin, C. Stampfer, A. Jungen, C. Hierold, L. Wirtz, Nano Lett. 7 (2007) 238.
[28] L.M. Malard, M.H.D. Guimarães, D.L. Mafra, M.S.C. Mazzoni, A. Jorio, Phys. Rev. B 79 (2009) 125426.
[29] Y. Hao, Y. Wang, L. Wang, Z. Ni, Z. Wang, R. Wang, C.K. Koo, Z. Shen, J.T.L. Thong, Small 6 (2010) 195.
[30] Y. Zhang, L. Gomez, F.N. Ishikawa, A. Madaria, K. Ryu, C. Wang, A. Badmaev, C. Zhou, J. Phys. Chem. Lett. 1 (2010) 3101.
[31] A. Das, S. Pisana, B. Chakraborty, S. Piscanec, S.K. Saha, U.V. Waghmare, K.S. Novoselov, H.R. Krishnamurthy, A.K. Geim, A.C. Ferrari, A.K. Sood, Nat. Nanotechnol. 3 (2008) 210.
[32] G. Tsoukleri, J. Parthenios, K. Papagelis, R. Jalil, A.C. Ferrari, A.K. Geim, K.S. Novoselov, C. Galiotis, Small 5 (2009) 2397.
[33] O. Frank, G. Tsoukleri, J. Parthenios, K. Papagelis, I. Riaz, R. Jalil, K.S. Novoselov, C. Galiotis, ACS Nano 4 (2010) 3131.
[34] M. Weser, Y. Rehder, K. Horn, M. Sicot, M. Fonin, A.B. Preobrajenski, E.N. Voloshina, E. Goering, Y.S. Dedkov, Appl. Phys. Lett. 96 (2010) 012504.
[35] A. Siokou, F. Ravani, S. Karakalos, O. Frank, M. Kalbac, C. Galiotis, Appl. Surf. Sci. 257 (2011) 9785.
[36] S. Sinharou, L.L. Levenson, Thin Solid Films 53 (1978) 31.
[37] Alloy phase Diagrams ASM Handbook, ASM International, vol. 3, 1992.
[38] I. Vlassiouk, M. Regmi, P. Fulvio, S. Dai, P. Datskos, G. Eres, S. Sergei, ACS Nano 5 (2011) 6069.
[39] F. Abild-Pedersen, J.K. Nørskov, J.R. Rostrup-Nielsen, J. Sehested, S. Helveg, Phys. Rev. B 73 (2006) 115419.
[40] S. Helveg, C. López-Cartes, J. Sehested, P.L. Hansen, B.S. Clausen, J.R. Rostrup-Nielsen, A.P. Frank, K.N. Jens, Nature 427 (2004) 426.
[41] C. Mattevi, H. Kim, M. Chhowalla, J. Mater. Chem. 21 (2011) 3324.
[42] K.L. Saenger, J.C. Tsang, A.A. Bol, J.O. Chu, A. Grill, C. Lavoie, Appl. Phys. Lett. 96 (2010) 153105.
[43] G. Ertl, H. Knozigner, F. Schuth, I. Weikamp, in: Handbook of Heterogeneous Catalysis 2nd Completely Revised and Enlarged Edition, Wiley – VCH, 2008, p. 1081.
[44] L. Baraton, Z. He, C.S. Lee, J.L. Maurice, C.S. Cojocaru, A.F.G. Lorenzon, Y.H. Lee, D. Pribat, Nanotechnology 22 (2011) 085601.